SAR True Digital Ortho Map Production for Target Geometric Structure Preservation

Niangang Jiao, Feng Wang, Yuxin Hu, Yuming Xiang, *Member, IEEE*, Rui Liu, and Hongjian You

***Abstract*—Geometric structural information of objects in synthetic aperture radar (SAR) images is of great significance in target detection and analysis. The existing orthorectification methods of SAR images generally follow the traditional routes of optical images, resulting in suffering from the influence of layover, and bring difficulties in image analysis or target extraction without sufficient prior knowledge. Therefore, this article proposes a highest-projection-principle-based SAR true digital ortho map (TDOM) production method for the restoration of geometric structural information of targets. First, ground control information extracted from the high-precision digital surface model is applied to calibrate the geolocation error of original SAR images. Second, the highest projection principle and the visibility detection are utilized to reduce the influence of layover. To preserve the structural information of targets, multiview SAR TDOMs are integrated and compensated to generate a fused SAR TDOM image similar to optical view. Two Gaofen-3 (GF-3) SAR spotlight images are included to verify the performance of our proposed method. Experimental results are compared qualitatively in visual effects and quantitatively in geolocation accuracy. The results indicate that the produced SAR TDOMs can preserve the structural information of targets and provide more similar geometric structural information as optical images, which will effectively improve the efficiency in the interpretation of orthorectified SAR images.**

***Index Terms*—Geometric structural information, layover area, synthetic aperture radar (SAR), true digital ortho map (TDOM).**

I. Introduction

SYNTHETIC aperture radar (SAR) using an active microwave sensor can provide earth observations in all weather and all day without cloud cover . Therefore, SAR images have been widely used in mapping, geology, and other fields [1]. Owing to the side-viewing and range imaging characteristics, geometric distortions, such as layover, always exist in SAR digital ortho maps (DOMs) after orthorectification [2], [3]. These distortions degenerate the structural information and bring difficulties for target recognition and interpretation [4].

The side-viewing geometry of SAR systems will lead to geometric distortions such as layover, and orthorectification is necessary to reduce these geometric distortions [5]. Nowadays, orthorectification of SAR images developed based on the rational function model (RFM) is widely applied in photogrammetric production considering the simplicity of implementation and standardization [6]. In 2012, Zhang et al. [7] analyzed the suitability of RFM in the orthorectification of SAR images. Later, Wang et al. [8] verified the efficiency of the RFM in block adjustment and orthorectification based on the spaceborne YG-5 SAR imagery. In 2020, Guo et al. [9] investigated the performance of integrated orthorectification of ZY-3 and Gaofen-3 (GF-3) images. Wang et al. [10] proposed a block orthorectification method without ground control points (GCPs) using large-scale GF-3 fine strip II mode SAR images. To remove the influence of layover, Zhang et al. [11] proposed a layover area determination method based on the relationship between the look angle and the slope angle in slant range direction. By analyzing the corresponding coordinates in layover areas, Wang et al. [12] proposed a probability-based method for layover detection and compensation during SAR orthorectification. Later, value-based methods were proposed for detection and compensation [13], [14], which were not robust enough. Most methods of SAR layover compensation are developed and tested in mountainous areas; seldom of them has investigated algorithms on the geometric structural information preservation in buildings and other artificial targets.

In comparison, true orthorectification of aerial optical images has attracted extensive attention to remove the projective deformation caused by building dislocation and obscuration and restore the structural information [15]. Detection of distortion areas and texture reparation are key technologies in aerial optical image true orthorectification. Based on the initially developed Z-buffer method [16], distortion areas can be detected with the help of digital surface model (DSM) and digital building model (DBM). Deng et al. [17] proposed an occlusion detection method based on the overall projection of the DBM. Shen et al. [18] proposed an image rectification method based on image consistency to reduce the influence of "ghosting." These methods are highly dependent on the existing DBMs that may not always be accessible.

Inspired by previous research on optical true digital ortho map (TDOM) production, this article aims at investigating SAR TDOM production to reduce the influence of layover phenomenon and restore the structural information of objects. To this end, the highest projection principle is applied to generate orthorectified SAR images in an optical view. First, the geometric parameters of original SAR images are corrected to eliminate the misalignment between SAR images and the reference

Manuscript received 27 March 2023; revised 13 July 2023 and 18 September 2023; accepted 20 October 2023. Date of publication 27 October 2023; date of current version 23 November 2023. *(Corresponding author: Feng Wang.)*

The authors are with the Key Laboratory of Technology in Geo-Spatial Information Processing and Application System, Aerospace Information Research Institute, Chinese Academy of Sciences, Beijing 100094, China (e-mail: jiaoniangang16@mails.ucas.ac.cn; fengwang@126.com; yuxinhu@163.com; yumingxiang@163.com; ruiliu@163.com; hongjianYou@163.com).

Digital Object Identifier 10.1109/JSTARS.2023.3328049

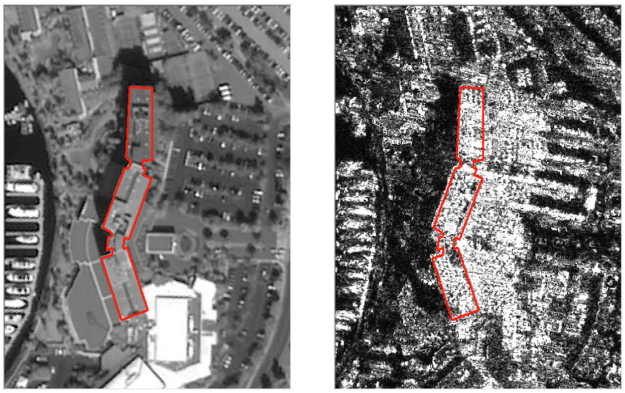

(a) (b)

Fig. 1. Comparison of SAR and optical images. (a) Optical image. (b) SAR image.

DSM. After calibration, object-space coordinates are projected into image space according to the imaging model of calibrated SAR images, and the multiprojected points in image space are detected as layover. To generate a single SAR TDOM image, the highest projection principle and the visibility detection are applied to build a proper projection relationship in layover areas. After morphological processing, multiview SAR TDOMs from compensated aspects are integrated together to recompense the blank area. The main contributions of this article are as follows.

1) A SAR TDOM production method is proposed to remove the distortions in layover area and restore the structural information of the target in orthorectified SAR images.
2) Layover areas in SAR images are detected based on the multiple projections between image space and object space.
3) Layovers in object space are unmixed to restore the object structural information, and distortions are reduced according to the highest projection principle and visibility detection in optical imaging systems.

The rest of this article is organized as follows. Section II gives the detailed description of the proposed SAR TDOM production method. The experimental results are presented and analyzed using GF-3 SAR images in Section III. Finally, Section IV concludes this article.

II. Mathematical Model

As shown in Fig. 1, it is still a hard work for most users to build accurate correlation between orthorectified optical and SAR images until now. The structural information from top view within the red rectangle in Fig. 1(a) can be clearly defined, while the building in Fig. 1(b) is greatly obscured by the existed layover. Therefore, this article aims to produce orthorectified SAR images sharing the same visual effect with optical images from the top view. To this end, algorithms in layover area detection and orthorectification in layover areas are investigated. Fig. 2 gives the workflow of our proposed method. First, original SAR images are calibrated with the help of high-precision DSMs to remove the misalignment. Then, object-space coordinates are projected into the calibrated SAR image space, and the layover areas are masked when the image-space coordinates are multiple projected. To preserve the target with clear structural information in SAR images, relationships between the object-space coordinate and image-space coordinate are determined one-to-one according to the highest projection principle and visibility detection. After projection, blank regions caused by multiple projections in layover area are compensated using images from different aspects. The compensated orthorectified SAR images share the same visual effects with optical images around the target, which can make SAR images more user-friendly and improve the efficiency in image interpretation.

A. Geometric Calibration

Limited by the measurement accuracy of onboard facilities, ground control information is necessary for geolocation error calibration. In view of the discrepancies between SAR images and DSM data, ground control information can be derived from a DSM-based simulated SAR image (DSSI) [19]. Therefore, it is much easier to extract tie points (TPs) from the simulated SAR image and the original SAR image, and TPs extracted from the simulated SAR image can be treated as GCPs to calibrate the geolocation error using an affine transformation-model-aided RFM [20]. The geolocation information of the DSM can be projected into a simulated SAR image based on the imaging model of SAR images, which share the same geolocation accuracy with the DSM and similar visual effect with the original SAR image. The geolocation model of SAR images is known as the range–Doppler (RD) model, which project a target in object space into image space by combining the measured range information and Doppler information. Usually, the RD model is defined as

$$\begin{cases} \sqrt{(X_s - X)^2 + (Y_s - Y)^2 + (Z_s - Z)^2} = R \\ V_x \cdot (X_s - X) + V_y \cdot (Y_s - Y) + V_z \cdot (Z_s - Z) = \frac{f_D \cdot \lambda \cdot R}{2} \end{cases} \tag{1}$$

where (X_S, Y_S, Z_S) and (X, Y, Z) are the position vector of the SAR sensor and the ground target, respectively, (V_x, V_y, V_z) represents the velocity vector of the SAR sensor, R is the measured range between the satellite SAR sensor and the target, f_D is the Doppler frequency, and λ is the wavelength.

To produce a simulated SAR image, the satellite position and velocity vector should be interpolated based on discrete records, so that every ground target can be projected to the simulated SAR image. After geometry projection, the radiometric characteristics for each image-space point should be determined.

Radiometric characteristic of SAR images gives the reflectance of ground targets, which is a combination of incidence angle, terrain, and various types of ground coverage. During the process, the type of ground coverage cannot be actually extracted and labeled based on the provided image information and assisted elevation information. Therefore, the texture in simulated SAR image is mainly determined by the incidence angle and terrain. And the elevation information should be resampled first to guarantee the consistency between the true SAR image and

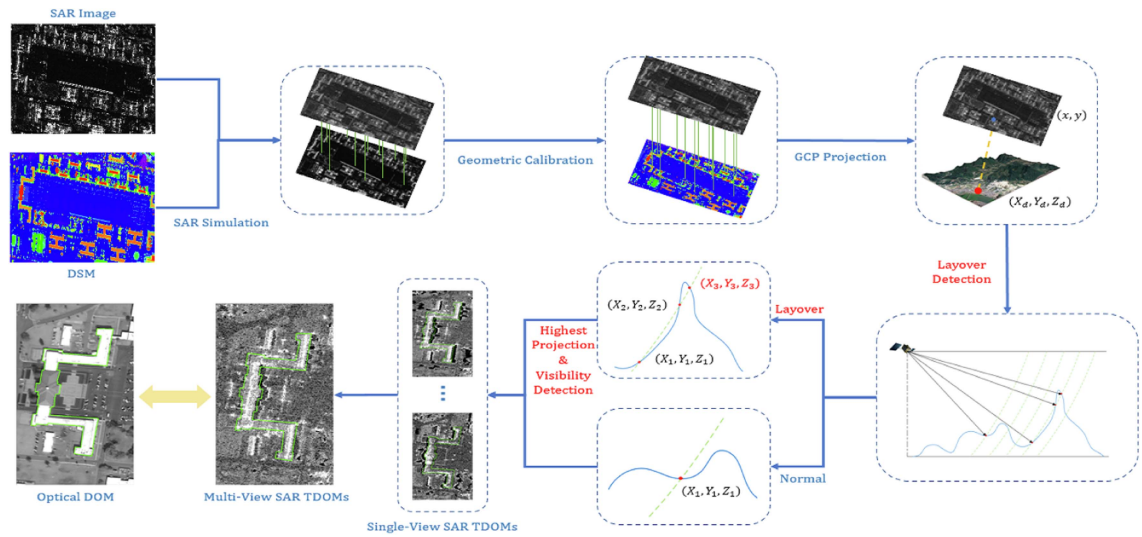

Fig. 2. Workflow of our proposed method.

the simulated SAR image according to the following equation:

$$f >= \frac{\delta_r}{\delta_{rg}} \frac{\sqrt{2}\Delta S_E}{\Delta S_{\text{SAR}}} = \sin\theta \frac{\sqrt{2}\Delta S_E}{\Delta S_{\text{SAR}}} \tag{2}$$

where δ_r and $\delta_r g$ are used to calculate the local incidence angle θ. Δ_E and Δ_{SAR} are the ground resolution of elevation information and SAR images, respectively.

After resampling, radiometric reflectance can be calculated for each location based on commonly used radar scattering models [21]

$$\sigma = \frac{0.133 \cdot \cos\theta}{\sin\theta + 0.1\cos\theta}. \tag{3}$$

To obtain a simulated SAR image sharing the same characteristics with the true SAR image, the ground resolution of the applied elevation information should be slightly higher than the true SAR image, so that the simulated SAR image can maintain sufficient texture information. With the decrease of the resolution, structural information in the DSSI will become gradually blurry. Moreover, the geolocation parameters of the provided true SAR image should be as higher as possible to guarantee the calibration accuracy.

Edge information, which is effective in the expression of geometric structural information, is usually utilized to build relationships between images. Therefore, we chose the phase-congruency-based SAR-PC model to extract proper edge responses from the DSSI and true SAR images [22]. To build the SAR-PC, the local energy E_{sar} and amplitude A_n should be calculated first as

$$\begin{aligned} E_{\text{sar}}(x,y) &= \sqrt{(\Sigma_n e_n(x,y))^2 + (\Sigma_n o_n(x,y))^2} \\ \Sigma_n A_n &= \Sigma_n \sqrt{(e_n(x,y))^2 + (o_n(x,y))^2} \end{aligned} \tag{4}$$

where n represents the scale, and e_n and o_n are the calculated Hilbert transform with the local means of μ_o and μ_e, respectively:

$$\begin{cases} \mu_o(x,y) = \Sigma_{x',y'} I(x',y') Go(x-x', y-y') \\ \mu_e(x,y) = \Sigma_{x',y'} I(x',y') Ge(x-x', y-y') \end{cases} \tag{5}$$

$$\begin{cases} e(x,y) = 1 - \min\frac{\mu_o^1}{\mu_o^2}, \frac{\mu_o^2}{\mu_o^1} \\ o(x,y) = \min(1 - \min\frac{\mu_e^1}{2\mu_e^2}, \frac{2\mu_e^2}{\mu_e^1}, 1 - \min\frac{\mu_e^1}{2\mu_e^3}, \frac{2\mu_e^3}{\mu_e^1}) \end{cases} \tag{6}$$

where $Go(x,y)$ and $Ge(x,y)$ are the even-symmetric and odd-symmetric Gabor filters, respectively.

Therefore, the SAR-PC can be derived as

$$PC_{\text{sar}} = \frac{\Sigma_o W_o(x,y) \lfloor E_{\text{sar}-o}(x,y) - T_{\text{sar}-o}(x,y) \rfloor}{\Sigma_o \Sigma_n A_n + \epsilon} \tag{7}$$

where o represents different orientation, W_o is the weight function of the oth orientation, T_{sar} is the estimated noise level, and ϵ is a small positive value to prevent the expression from becoming unstable when A_n becomes very small.

To build the geometric relationships between the DSSI and true SAR images based on the extracted edge information, we applied the normalized cross correlation (NCC) matching method to build TPs as

$$R = \frac{\Sigma_{x,y}(I_1(x,y) - \mu_1)(I_1(x+dx, y+dy) - \mu_2)}{\sqrt{\Sigma_{x,y}(I_1(x,y) - \mu_1)^2 + \Sigma_i (I_2(x+dx, y+dy) - \mu_2)^2}} \tag{8}$$

where (x,y) and (dx,dy) represent the image-space coordinates in the simulated SAR image I_1 and the offsets between the simulated and true SAR image I_2. μ_1 and μ_2 are the mean values of the simulated and SAR images, respectively.

B. SAR TDOM Production

Traditional produced SAR images suffer from distortions with layover, foreshortening, and shadow, among which the layover greatly destroyed the structural information of the target. Echo

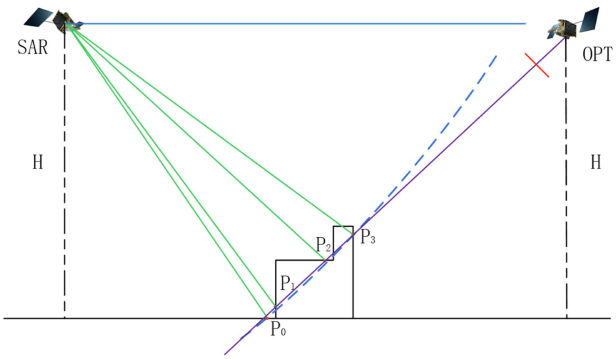

Fig. 3. Illustration of layover unmixing for SAR TDOM production.

data from different objects will be projected into the same image-space coordinates, which mixed the signals from more than one target, including the ground, the side, and the top of the target. Traditionally, the mixed information is considered as a whole and compensated using information from compensated perspectives. These methods throw away all information existing in the layover area, and the final results depend on the complementarity of multiview datasets. To unmix the aliased signals, we try to project the received signal to a proper locate referring to the production algorithms of optical TDOM, which can clearly express the structural characteristics of the target.

Assuming that the totally l objects with coordinates $P_i(X_i, Y_i, Z_i)(i = 0, 1, \ldots, l)$ are projected into the same image-space coordinate $p(x, y)$ in original SAR images, we can build the relationship using the calibrated RFM as

$$\begin{cases} x = \dfrac{\Sigma_{i=0}^{3}\Sigma_{j=0}^{3}\Sigma_{k=0}^{3} a_{ijk} X_0^i Y_0^j Z_0^k}{\Sigma_{i=0}^{3}\Sigma_{j=0}^{n2}\Sigma_{k=0}^{3} b_{ijk} X_0^i Y_0^j Z_0^k} \\ y = \dfrac{\Sigma_{i=0}^{3}\Sigma_{j=0}^{3}\Sigma_{k=0}^{3} c_{ijk} X_0^i Y_0^j Z_0^k}{\Sigma_{i=0}^{3}\Sigma_{j=0}^{n2}\Sigma_{k=0}^{3} d_{ijk} X_0^i Y_0^j Z_0^k} \\ \cdots \\ x = \dfrac{\Sigma_{i=0}^{3}\Sigma_{j=0}^{3}\Sigma_{k=0}^{3} a_{ijk} X_l^i Y_l^j Z_l^k}{\Sigma_{i=0}^{3}\Sigma_{j=0}^{n2}\Sigma_{k=0}^{3} b_{ijk} X_l^i Y_l^j Z_l^k} \\ y = \dfrac{\Sigma_{i=0}^{3}\Sigma_{j=0}^{3}\Sigma_{k=0}^{3} c_{ijk} X_l^i Y_l^j Z_l^k}{\Sigma_{i=0}^{3}\Sigma_{j=0}^{n2}\Sigma_{k=0}^{3} d_{ijk} X_l^i Y_l^j Z_l^k} \end{cases} \tag{9}$$

where (x, y) denote the row and col index in image space, respectively. (X, Y, Z) are the normalized geodetic longitude, latitude, and height in object space, respectively. (a, b, c, d) are the coefficients of the RFM. (i, j, k) represent the order of the coefficients.

To detect the accurate location of layover area in image spaces, the sampling rate in image space is calculated. First, the visibility of the object is detected with the slope and aspect information obtained from the DSM. For the layover area in visible regions, signals from more than one object were received at the same time. That means, when we project the image point into object space, the projection solutions will not convergence or oscillated between several results. Otherwise, the projection can converge to only one result.

As shown in Fig. 3, the blue line and the purple line represent the imaging plane of the SAR sensor and the equivalent optical sensor with the same orbit height H, respectively. The green line indicates that the measurement distances from objects P_0–P_3 are the same, and the blue dotted line is part of the equidistant line. The purple line is the line of sight from the equivalent optical sensor. Zhang et al. [7] have already analyzed the feasibility of the RFM in orthorectification of satellite SAR images, which means that differences between the blue line and the purple line can be neglected.

Based on the provided geolocation model, we can calculate the coverage of the projected SAR images, and the corresponding geometric transformation model between the projected image-space coordinate $(x_{\text{proj}}, y_{\text{proj}})$ and the geodetic coordinate (Lon, Lat). The equation can be shown as

$$\begin{cases} x_{\text{proj}} = \dfrac{Adf_6 \cdot (Lon - Adf_1) - Adf_3 \cdot (Lat - Adf_4)}{Adf_2 * Adf_6 - Adf_3 * Adf_5} \\ y_{\text{proj}} = \dfrac{Adf_2 \cdot (Lat - Adf_4) - Adf_5 \cdot (Lon - Adf_1)}{Adf_2 * Adf_6 - Adf_3 * Adf_5} \end{cases} \tag{10}$$

where $Adf_i (i = 1, 2, \ldots, 6)$ represent the coefficients of the geometric transformation model. By combining (9) and (10), we can build the relationships of image-space coordinates between projected SAR images and original SAR images.

During the geocoding process, ground targets with geodetic coordinates can be detected in the projected SAR image using (10). At the same time, the image-space coordinates in original SAR images can be calculated by the RFM in (9). Owing to the imaging geometry in SAR images, image-space points in original SAR images located in layover areas are mixed with echo from multiple ground targets. As shown in Fig. 3, objects from $P_0(X_0, Y_0, Z_0) \sim P_3(X_3, Y_3, Z_3)$ projected to $p(x, y)$ successively, and the object-space coordinates are sorted by elevation. Based on the results of visibility detection, P_3 was excluded first. Assuming that $Z_0 < Z_1 < Z_2$, the image-space coordinate p is projected to the highest object P_2, where P_0 and P_1 are neglected. During the resample of orthorectification, the corresponding points of P_2 are interpolated with the pixel value from p, while P_0 and P_1 are filled with a no-data value. The single SAR TDOM image can be produced with the proper projection relationships.

The produced single SAR TDOM can clearly give the structural information of the target with a pseudo optical view. Areas filled with no-data value often presented as blank due to the truncation of multiprojections, which influence the visual effect of the SAR TDOM. Therefore, different SAR TDOMs are fused together by the radiometric-principle-based radiometric normalization method [23].

III. Experimental Results and Analysis

A. Tested Datasets

SAR images obtained from the GF-3 satellite and the light detection and ranging (LiDAR)-derived DSM around the San Diego International Airport in America are experimented, as shown in Fig. 4. The DSM was produced from an airborne LiDAR system. The ground resolution of the resampled DSM is 0.5 m, and the accuracy is higher than 20 cm. The nominal resolution of SAR images is 1 m. Table I gives the detailed information of the experimental SAR images.

(a) (b) (c)

Fig. 4. Experimental datasets. (a) Overview of the DSM. (b) and (c) are the thumbnail of two experimented SAR images. (a) DSM. (b) GF3-358. (c) GF3-552.

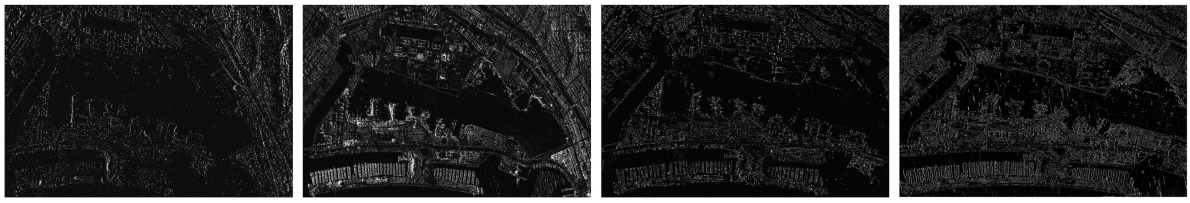

(a) (b) (c) (d)

Fig. 5. Experimental datasets. (a) and (b) are DSM-simulated SAR image and the true SAR image. (c) and (d) show the corresponding edge information. (a) DSSI image. (b) GF3-358 SAR image. (c) Edge extracted from the DSSI image. (d) Edge extracted from the GF3-358 SAR image.

TABLE I
DETAILED INFORMATION OF GF-3 SAR IMAGES

No.	Mode	Incident Angle	Orbit	Look Direction	Average Terrain
GF3-358	SL	34.00°	DEC	R	38.88 m
GF3-552	SL	41.17°	ASC	R	2.68 m

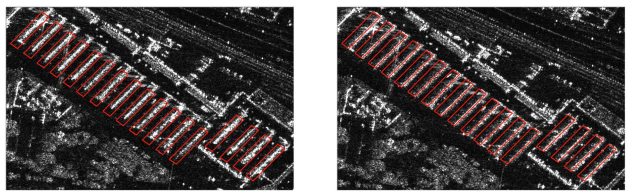

(a) (b)

Fig. 6. Comparison of the discrepancies (a) before and (b) after calibration.

TABLE II
GEOMETRIC ACCURACY OF SAR IMAGES BEFORE AND AFTER CALIBRATION (M)

No.	Before Calibration			After Calibration		
	X	Y	P	X	Y	P
GF3-358	25.84	11.91	28.45	0.85	0.33	0.92
GF3-552	28.92	10.83	30.88	0.96	0.42	1.03

B. TDOM Production

First, the DSSI image is utilized to extract control information for the calibration of raw SAR images. As shown in Fig. 5(a) and (b), the DSSI and true SAR images shows similarity in geometric characteristics. In contrast, the radiometric performance varies greatly between the DSSI and true SAR images due to the lack of a priori scattering properties of the ground surface. Therefore, the edge information that can effectively express the geometric structural features is utilized to build relationships between the DSSI and true SAR images. Based on the results shown in Fig. 5(c) and (d), TPs can be extracted using the NCC matching method, and the raw SAR images can be calibrated based on the control information extracted from the DSSI.

Fig. 6(a) and (b) shows the discrepancies between the reference vectors and the original SAR images before calibration. The red contours are the OpenStreetMap vectors of the buildings [24], sharing the geometric consistency with the DSM. Ground control information is extracted to calibrate the geometric error of SAR images. After correction, the geometric consistency between SAR images and the DSM is greatly improved, as shown in Fig. 6(b). Table II gives the geometric performance before and after calibration with the DSM. The geolocation accuracy of two SAR images was improved from about 30 to within 1 m, which can satisfy our requirements for SAR TDOM production.

Three scenarios, including the MCRD Museum (area 1), the Sheraton Hotel (area 2), and the Airport Authority Administration (area 3) around the San Diego International Airport are included to compare the visual effect of the produced TDOM and traditional DOM. Fig. 7 gives the results of the MCRD San Diego Museum building. Edge details of the building in Fig. 7(a) and (g) are greatly stretched and mixed with the ground in the direction of facing the wave, which is hard to be detected. In contrast, the building is separated from the ground in Fig. 7(d) and (j). The structural of the building can be easily detected and

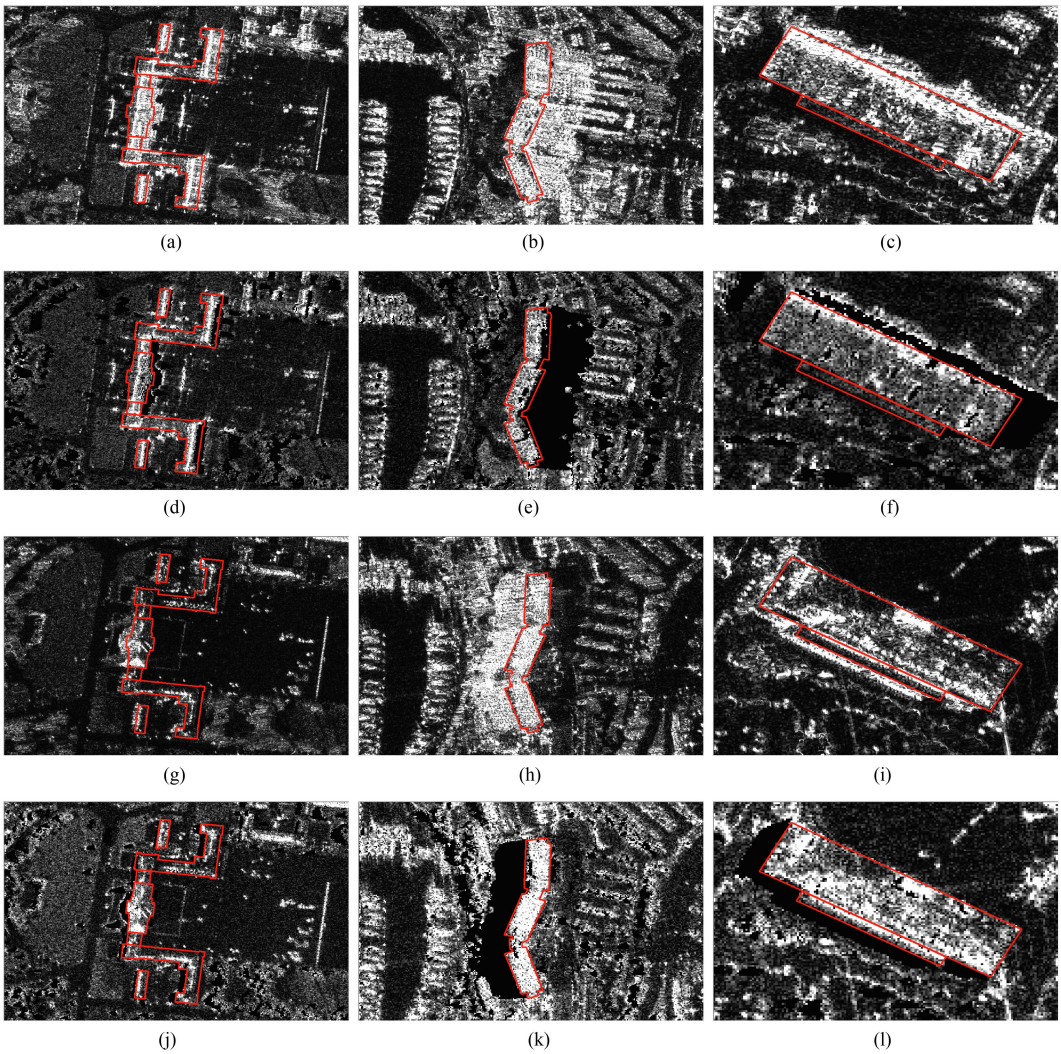

Fig. 7. Comparison of the produced SAR DOMs and SAR TDOMs. The first column shows the results in the MCRD Museum, the second column shows the results in the Sheraton Hotel, and the third column shows the result in the Airport Authority Administration. (a) GF3-358 DOM in area 1. (b) GF3-358 DOM in area 2. (c) GF3-358 DOM in area 3. (d) GF3-358 TDOM in area 1. (e) GF3-358 TDOM in area 2. (f) GF3-358 TDOM in area 3. (g) GF3-552 DOM in area 1. (h) GF3-552 DOM in area 2. (i) GF3-552 DOM in area 3. (j) GF3-552 TDOM in area 1. (k) GF3-552 TDOM in area 2. (l) GF3-552 TDOM in area 3.

identified, and the blank areas are considered as shadows from an optical view.

Similarly, the second and third columns in Fig. 7 give the comparison of the produced SAR DOM and SAR TDOM in the Sheraton Hotel and the Airport Authority Administration. In traditional produced SAR DOMs, the existing layovers mixed the structural information of the target and the ground together. The edge information and structural information are hard to be distinguished in these images. In contrast, the produced SAR TDOMs draw the outline of the target from a top view clearly. The caused layover in original SAR images is compressed into the edge of the object, making the boundary easier to be identified.

In the produced single SAR TDOMs, blank areas in the direction facing the wave always affect the visual effect and lost some information in the surrounding areas of the targets. Therefore, the multiview images are fused and compensated to show the full view of the target area. Fig. 8(a)–(f) gives the comparison of the fused SAR TDOMs and the DSM of different buildings. The fused results are produced by compensate the blank area in GF3-358 and GF3-552 with each other. Lost information in the direction facing the wave is compensated using complementary images. Both the geometric structural information and the surroundings are clearly identified, which gives a similar visual effect as the optical images. It should be noted that when we conduct the compensation process, the selected SAR TDOMs should have complementary side-viewing information (e.g., one image looking from the left side and the other looking from the right side), so that lost information in one image in layover areas can be obtained by another one. Another key point is that the viewing angle of two compensated SAR images should be as equal as possible, so that the compensated area can give the similar geometric performance with each other.

To quantitatively evaluate the performance of our proposed method, the similarity between DSM and the fused SAR TDOMs was calculated. Table III gives the comparison of traditional SAR

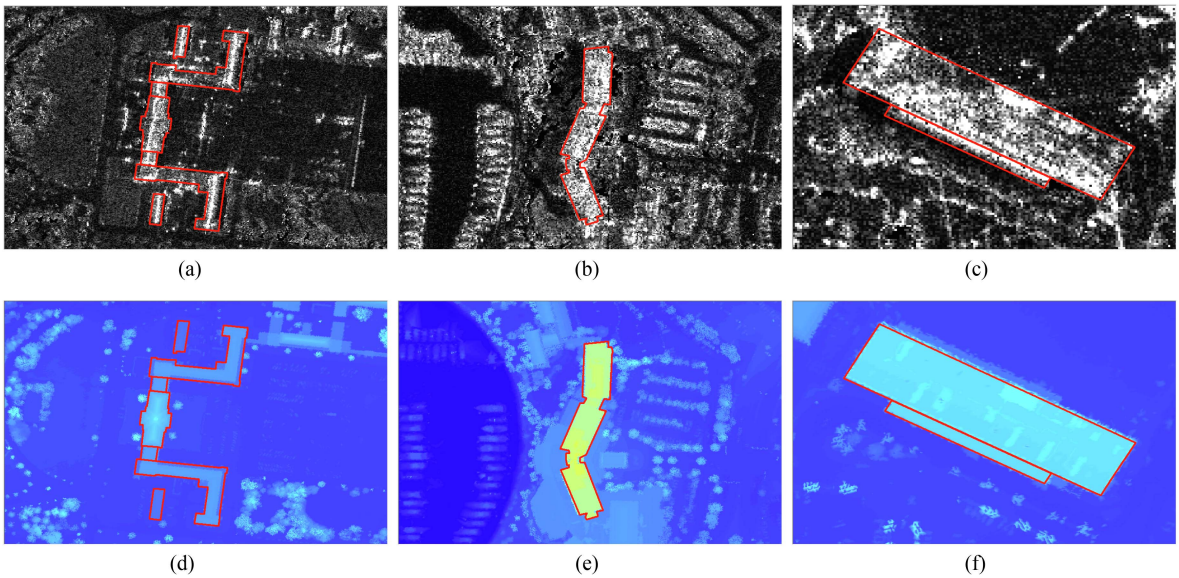

Fig. 8. Comparison of the fused TDOMs and the relevant DSMs. (a) Fused TDOM in area 1. (b) Fused TDOM in area 2. (c) Fused TDOM in area 3. (d) DSM in area 1. (e) DSM in area 2. (f) DSM in area 3.

TABLE III
GEOMETRIC SIMILARITY EVALUATION BETWEEN DIFFERENT SAR PRODUCTS AND THE DSM

	test area 1	test area 2	test area 3
SAR TDOM	94%	95%	92%
SAR DOM	88%	86%	87%

DOMs and our proposed SAR TDOMs. The NCC is applied here again to verify the scenario consistency of the whole tested area. Owing to the influence of layover phenomenon, traditional SAR DOMs are much brighter than optical area in the direction facing to the sensor. In contrast, our fused SAR TDOMs can give more clear structural information of the target. As we can see, the geometric similarity between SAR TDOMs and DSM is about 8% higher than that between SAR DOMs and DSM in all three scenarios, especially in areas with tall buildings. Therefore, the produced SAR TDOMs share more similarity with optical sensors for easier interpretation.

Totally, our proposed method can efficiently produce SAR TDOMs with clear geometric structural information, which gives a similar view as the optical images. Therefore, distortions in layover areas are effectively eliminated, and targets in the produced SAR TDOM are easily detected and analyzed.

IV. CONCLUSION

Aiming at producing SAR orthoimages with clearly structural information, this article investigated the SAR TDOM production method based on the highest projection principle. Original SAR images are calibrated using reference DSM, and the layover areas are detected and masked when more than one objects are projected to the same image-space coordinates. Once the layover areas are masked, the highest projection principle and the visibility detection are applied to unmix the miscellaneous signals into the proper objects. Based on the developed projection relationships one-by-one, the SAR TDOMs can be produced with clearly boundary separated from the ground. Multiview SAR TDOMs are fused together to obtain the objects with the same visual effect as optical images. Our proposed fused SAR TDOMs show better understanding and visual connection to the optical world, thereby providing a better way for SAR orthoimages understanding and analysis.

REFERENCES

[1] M. Ottinger and C. Kuenzer, "Spaceborne L-band synthetic aperture radar data for geoscientific analyses in coastal land applications: A review," *Remote Sens.*, vol. 12, no. 14, 2020, Art. no. 2228.
[2] X. Chen, Q. Sun, and J. Hu, "Generation of complete SAR geometric distortion maps based on DEM and neighbor gradient algorithm," *Appl. Sci.*, vol. 8, no. 11, 2018, Art. no. 2206.
[3] L. Wu, H. Wang, Y. Li, Z. Guo, and N. Li, "A novel method for layover detection in mountainous areas with SAR images," *Remote Sens.*, vol. 13, no. 23, 2021, Art. no. 4882.
[4] Y. Sun, L. Mou, Y. Wang, S. Montazeri, and X. X. Zhu, "Large-scale building height retrieval from single SAR imagery based on bounding box regression networks," *J. Photogrammetry Remote Sens.*, vol. 184, pp. 79–95, 2022.
[5] Y. Sheng and D. Alsdorf, "Automated georeferencing and orthorectification of Amazon basin-wide SAR mosaics using SRTM DEM data," *IEEE Trans. Geosci. Remote Sens.*, vol. 43, no. 8, pp. 1929–1940, Aug. 2005.
[6] M. Soliman, H. Hamza, H. Elhifnawy, A. Ragab, and A. Elsharkawy, "Assessment of geometric correction of remote sensing satellite images using RPC versus GCP," *J. Eng. Sci. Mil. Technol.*, vol. v, no. 2, pp. 82–89, 2018.
[7] G. Zhang, Q. Qiang, Y. Luo, Y. Zhu, H. Gu, and X. Zhu, "Application of RPC model in orthorectification of spaceborne SAR imagery," *Photogrammetric Rec.*, vol. 27, no. 137, pp. 94–110, 2012.
[8] T. Wang et al., "Planar block adjustment and orthorectification of chinese spaceborne SAR YG-5 imagery based on RPC," *Int. J. Remote Sens.*, vol. 39, no. 3, pp. 640–654, 2018.
[9] L. Guo, X. Wang, and M. Yue, "Improved digital orthorectification map generation approach using the integrating of ZY3 and GF3 image," in *Proc. IEEE 5th Int. Conf. Image, Vis. Comput.*, 2020, pp. 82–85.

[10] T. Wang et al., "Large-scale orthorectification of GF-3 SAR images without ground control points for China's land area," *IEEE Trans. Geosci. Remote Sens.*, vol. 60, 2022, Art. no. 5221617.
[11] J. Zhang, J. Wei, G. Huang, and Y. Zhang, "Fusion of ascending and descending polarimetric SAR data for color orthophoto generation," in *Proc. ISPRS Tech. Commission VII Symp.*, 2010, pp. 323–328.
[12] H. Wang et al., "Layover compensation method for regional spaceborne SAR imagery without GCPs," *IEEE Trans. Geosci. Remote Sens.*, vol. 59, no. 10, pp. 8367–8381, Oct. 2021.
[13] B. Guindon and M. Adair, "Analytic formulation of spaceborne SAR image geocoding and "value-added" product generation procedures using digital elevation data," *Can. J. Remote Sens.*, vol. 18, no. 1, pp. 2–12, 1992.
[14] *Interferometric SAR Processor j ISP, Documentation j User's Guide, Version 1*, GAMMA Remote Sensing AG, Gümligen, Switzerland, 2010.
[15] M. Shariat, A. Azizi, and M. Saadatseresht, "Analysis and the solutions for generating a true digital ortho photo in close range photogrammetry," *Int. Arch. Photogrammetry, Remote Sens., Spatial Inf. Sci*, vol. 37, pp. 439–422, 2008.
[16] F. Amhar, J. Josef, and C. Ries, "The generation of true orthophotos using a 3D building model in conjunction with a conventional DTM," *Int. J. Photogrammetry Remote Sens.*, vol. 32, no. 4, pp. 16–22, 1998.
[17] F. Deng, P. Li, Y. Kan, J. Kang, and F. Wan, "Overall projection of DBM for occlusion detection in true orthophoto generation," *Geomatics Inf. Sci. Wuhan Univ.*, vol. 42, no. 1, pp. 97–102, 2017.
[18] C. Shen, L. Xu, and M. Xuwen, "Real projective processing of UAV based on image consistency detection," *Bull. Surveying Mapping*, no. 12, pp. 105–108, 2018.
[19] M. Shimada, "Ortho-rectification and slope correction of SAR data using DEM and its accuracy evaluation," *IEEE J. Sel. Topics Appl. Earth Observ. Remote Sens.*, vol. 3, no. 4, pp. 657–671, Dec. 2010.
[20] Y. Xiang, F. Wang, and H. You, "An automatic and novel SAR image registration algorithm: A case study of the Chinese GF-3 satellite," *Sensors*, vol. 18, no. 2, 2018, Art. no. 672.
[21] D. O. Muhleman, "Radar scattering from Venus and Moon," *Astronomic J.*, vol. 69, no. 5, pp. 34–40, 1964.
[22] Y. Xiang, F. Wang, L. Wan, and H. You, "SAR-PC: Edge detection in SAR images via an advanced phase congruency model," *Remote Sens.*, vol. 9, no. 3, 2017, Art. no. 209.
[23] R. Liu, F. Wang, N. Jiao, W. Yu, H. You, and F. Liu, "Radiometric principle-based radiometric normalization method for SAR images mosaic," *IEEE Geosci. Remote Sens. Lett.*, vol. 19, 2022, Art. no. 4509905.
[24] "Openstreetmap." Accessed: Jan. 11, 2023. [Online]. Available: https://www.openstreetmap.org/#map=13/32.7258/-117.1230

Niangang Jiao received the B.S. degree in electronic and information engineering from Shandong University, Jinan, China, in 2016, and the Ph.D. degree in information and signal processing from Aerospace Information Institute, Chinese Academy of Sciences, Beijing, China, in 2021.

He is currently an Assistant Researcher with the Key Laboratory of Technology in Geo-Spatial Information Processing and Application System, Aerospace Information Institute, Chinese Academy of Sciences. His research interests include multisource remote sensing image preprocessing, geometric and radiometric correction, and image mosaicing.

Feng Wang received the B.S. degree in photoelectric information engineering from the Beijing University of Aeronautics and Astronautics, Beijing, China, in 2010, and the Ph.D. degree in signal and information processing from the Chinese Academy of Sciences, Beijing, in 2015.

He is currently an Associate Researcher with Aerospace Information Research Institute, Chinese Academy of Sciences. His research interests include multisource remote sensing image processing, image registration, and change detection.

Yuxin Hu received the B.S. degree in communication engineering from Mongolian University, Hohhot, China, in 2002, and the Ph.D. degree in signal and information processing from the Institute of Electronics, Chinese Academy of Sciences, Beijing, China, in 2007.

He is currently a Professor with the Aerospace Information Research Institute, Chinese Academy of Sciences. His research interests include remote sensing satellite ground systems, remote sensing information processing, and spatial information processing system architecture.

Yuming Xiang (Member, IEEE) received the B.S. degree in electronic engineering from Tsinghua University, Beijing, China, in 2013, and the Ph.D. degree in signal and information processing from the Institute of Electronics, Chinese Academy of Sciences, Beijing, in 2018.

He is currently an Associate Researcher with the Key Laboratory of Technology in Geo-Spatial Information Processing and Application System, Aerospace Information Research Institute, Chinese Academy of Sciences. His research interests include remote sensing image registration and 3-D reconstruction.

Rui Liu received the B.S. degree in electronic information science and technology from Central South University, Changsha, China, in 2019. He is currently working toward the Ph.D. degree in signal and information processing with the Key Laboratory of Technology in Geo-Spatial Information Processing and Application Systems, Aerospace Information Research Institute, Chinese Academy of Sciences, Beijing, China.

His research interests include geometry processing of spaceborne synthetic aperture radar (SAR) image, radiometric normalization, and seamless SAR image mosaicking.

Hongjian You received the B.S. degree in engineering from Wuhan University, Wuhan, China, in 1992, the M.S. degree in surveying and mapping from Tsinghua University, Beijing, China, in 1995, and the Ph.D. degree in geography from the University of Chinese Academy of Sciences, Beijing, in 2001.

He is currently a Professor with the Key Laboratory of Technology in Geo-Spatial Information Processing and Application System, Aerospace Information Research Institute, Chinese Academy of Sciences, Beijing. His main research interests include remote sensing image processing and analysis, and synthetic aperture radar image applications.